文章编号：1001-9014(2019)06-0683-07

DOI:10.11972/j.issn.1001-9014.2019.06.001

Terahertz power amplifier integrated with on-chip antenna using GaN TMIC technology

WANG Xu-Dong[1,2], LV Xin[1], GUO Da-Lu[1], LI Ming-Xun[1], CHENG Gong[1], LIU Jia-Shan[1], YU Wei-Hua[1*]

(1. School of Information and Electronics, Beijing Institute of Technology, Beijing 100081, China;
2. Hebei Semiconductor Research Institute, Shijiazhuang 050051, China)

Abstract: This paper presents a transmitter-type TMIC integrated with a rectangular microstrip patch antenna and a power amplifier. The TMIC was fabricated with GaN HEMT technology for high power density and efficient integration. The on-chip antenna was designed as a power radiator and a frequency-dependent output load tuner of the power amplifier. Load-pull technique was used to realize a good impedance match between the amplifier and the antenna. Over a bandwidth of 100~110 GHz, the power amplifier can deliver an average output of 25.2 dBm with a power-added efficiency (PAE) of 5.83%. Good radiation characteristics of the TMIC have been achieved, showing a 10-dB bandwidth of 1.5 GHz and an estimated equivalent isotropic radiated power (EIRP) of 25.5 dBm at 109 GHz.

Key words: TMIC technology, GaN HEMT, active integrated antenna, radiation pattern

PACS: 84.40.Dc, 85.30.-z

基于GaN TMIC集成片上天线技术的太赫兹功率放大器

王旭东[1,2], 吕 昕[1], 郭大路[1], 李明迅[1], 程 功[1], 刘嘉山[1], 于伟华[1*]

(1. 北京理工大学 毫米波与太赫兹技术北京市重点实验室,北京 100081;
2. 河北半导体研究所,河北 石家庄 050051)

摘要:介绍了一种由矩形微带贴片天线和功率放大器一体化集成设计的发射类型单片太赫兹集成电路.该电路采用 GaN HEMT 工艺制备,实现了高功率密度和高效集成.片上天线被设计为功率放大器输出端接的功率辐射器和频率相关的输出负载调谐器.采用负载牵引技术实现了放大器与天线之间良好的阻抗匹配.在100~110 GHz的频带范围内,功率放大器的平均输出功率为25.2 dBm,平均功率附加效率(PAE)为5.83%.单片太赫兹集成电路具有良好的辐射特性,芯片的10 dB带宽为1.5 GHz,在109 GHz估算的等效各向同性辐射功率(EIRP)为25.5 dBm.

关 键 词:单片太赫兹集成电路技术;氮化镓高电子迁移率晶体管;有源集成天线;辐射方向图

中图分类号:O43 **文献标识码**:A

Introduction

Terahertz power radiation plays an important role in the fields of phased-array radar and wireless communication systems[1]. Most system applications require much more power than which is available or expected from a single device.

One way to achieve higher output power is based on planar power combining of discrete devices. In this approach, multi-stage amplification circuit cascading in parallel is the most common way to increase the output power[2]. With the increasing scale of cascade structures in this aggregation method, the insertion loss associated with increased cascade levels is rising at a very high rate, and the combining efficiency becomes unacceptable. The spatial power combining method, on the contrary, is expected to realize higher output power through electromagnetic wave superposition of free space propaga-

Received date: 2019-06-05, **revised date**: 2019-09-15 **收稿日期**:2019-06-05,**修回日期**:2019-09-15

Foundation items: Supported by National Natural Science Foundation of China (61527805).

Biography: WANG Xu-Dong(1986-), male, Hebei, China, Ph. D. Research area involves terahertz device, circuit and package for power combining. E-mail: wangxudong@bit.edu.cn

* **Corresponding author**: E-mail: ywhbit@bit.edu.cn

tion modes. High efficiency integration of large scale arrays can be achieved through quasi-optical technology [3].

In order to raise spatial power combining efficiency, it is necessary to reduce the transmission loss of each single device. To overcome this disadvantage, active integrated antenna (AIA) concept shown in Fig. 1 was proposed [4-7]. The AIA is defined as active circuits associated with antennas or antennas integrated with active components, which provides good radiation efficiency and compact size. The general AIA is composed of the power amplifier, output matching network of the power amplifier, even/odd harmonic tuning circuit of the power amplifier, antenna matching network and the antenna. Using a conventional active-antenna design, Qin *et al.* [8] reported a high-efficiency active antenna with a class-E power amplifier. A power amplifier with an 82.1% PAE and a 22.08-dBm output power was fabricated [8]. However, additional output matching network of the power amplifier is always needed for impedance matching with an antenna, which causes the increase of size and insertion loss and the decrease of PAE for the AIA system. The PAE was reduced to about 60% by integrating it with an antenna. Therefore, a study on the direct impedance matching between the power amplifier and antenna is required. Figure 2 shows the active integrated antenna configuration proposed in this paper. This configuration consists of a power amplifier, matching networks and an antenna. It is a simpler structure than conventional active antenna.

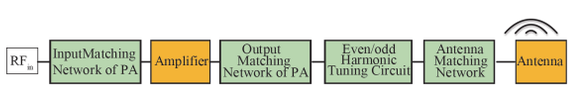

Fig. 1 Conventional active integrated antenna configuration[9]
图1 传统的有源集成天线框架图[9]

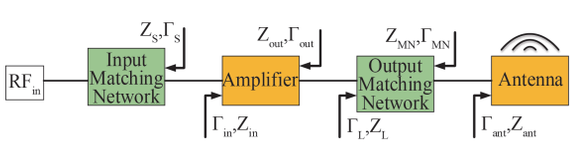

Fig. 2 Proposed active integrated antenna configuration
图2 本文的有源集成天线框架图

AIA systems using GaAs and SiGe MMIC technology are proposed in Refs. 10-12. However, poor power performances of GaAs and SiGe materials at high frequency limit their applications. Compared to SiC device, the heterogeneous structure significantly improves the electron mobility in the GaN material and brings a better high-frequency performance. By introducing GaN-on-SiC technology, GaN HEMT is exhibiting high power density coupled with good thermal conductivity, which has opened up the possibilities for highly efficient power amplifier integrating with on-chip antenna designs.

High-power AIA systems also require appropriate integration with a heat-cooling system. Large-signal characteristics, such as output power, PAE, and gain of the integrated amplifier are reduced by thermal effects. For instance, Wang *et al.* reported a PAE reduction of up to 17% between temperature of -55℃, 25℃, and 175℃ in a large signal modeling of a GaN HEMT[13]. Hence, it is necessary for a cooling system to adopt the material with good heat dissipation performance.

In this paper, the GaN TMIC technology was proposed to design a high-power transmitter front-end using the direct integration of the amplifier and the antenna. A load-pull technique was utilized to accurately evaluate impedances of the amplifier and design an impedance matching network between the amplifier and the antenna. A rectangular microstrip patch antenna was connected with the amplifier directly, allowing it to serve as a power radiator and a load tuner, thus minimizing circuit size and insertion loss.

1 Design

1.1 Analysis of Power Amplifier

Over the past years, GaN HEMT high-efficiency power-amplifiers have been investigated and realized via ways and means from optimizing the nonlinear active devices[14-16]. In order to realize high power radiation, the effective impedance matching between the amplifier and the antenna is essential.

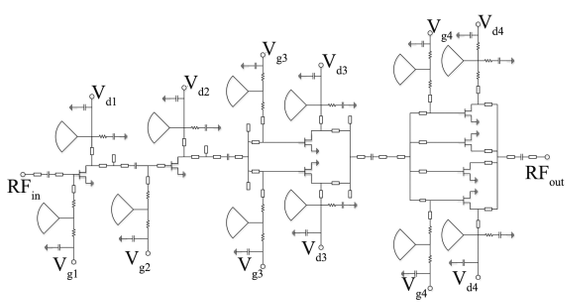

Fig. 3 Simplified topology of the terahertz-band GaN HEMT power amplifier
图3 太赫兹频段氮化镓高电子迁移率晶体管功率放大器拓扑结构示意图

Figure 3 shows the schematic of the terahertz band GaN HEMT power amplifier. This class-AB amplifier was designed and optimized using a Keysight Advanced Design System (ADS) Simulator. A four-stage schematic is designed to improve gain by optimizing gate width ratio among stages. Single-finger, two-finger and four-finger HEMT devices are used for the first two stages, the third stage and the final stage, separately. Each stage was designed to have a separate gate and drain bias pad. RF shorts employed quarter-wave shunt stubs to provide bias to the transistors. Shunt RC networks and radial stubs are included in the bias circuitry to maintain amplifier stability. Additionally, the ground coplanar waveguide (GCPW) structure is used in the input port to make the test easy and convenient. All the passive elements were separately modeled using the ADS Momentum electromagnetic (EM) simulation tool.

The TMIC was probed "on wafer" using two probe stations. A signal generator (Keysight 8257D) was used to generate signal centered at 18.3 GHz. The generated

signal was fed to the frequency extender (VDI E8257DV10) which multiplied the input signal from 18.3 GHz to 110 GHz. The simulated and measured small-signal *S*-parameters are shown in Fig. 4.

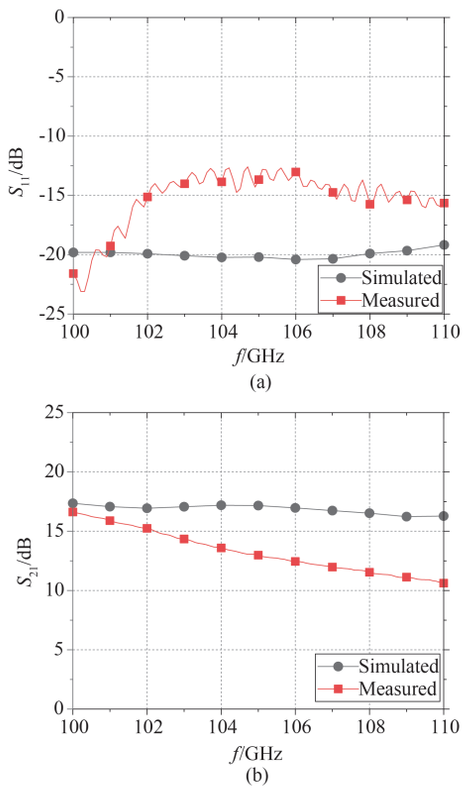

Fig.4　Small signal *S* parameter of GaN HEMT power amplifier (a) Small-signal parameter of S_{11}, and (b) small-signal parameter of S_{21}
图4　小信号 GaN HEMT 功率放大器 *S* 参数(a)小信号 S_{11} 参数,(b)小信号 S_{21} 参数

At 110 GHz, the output power (P_{out}) and PAE are measured and calculated as large-signal characteristics. The simulated and measured results are shown in Figs. 5-6. According to this measurement, the amplifier is operated with an +18 V drain voltage and a -2.5 V gate voltage. The measured results agree with the simulated values. The measured average output power is 25.2 dBm (330 mW) at an input of 19 dBm (80 mW). The average PAE is 5.83%. Under these conditions, an average power gain of 6.2 dB is confirmed.

1.2　Analysis of on-chip antenna

In this paper, a rectangular-microstrip-patch-antenna (RMPA) stands out among many different antenna types for three main reasons. Firstly, its good consistency helps to design and fabricate. Secondly, it is much easier to cascade with the amplifier. Thirdly, its radiation direction is along the positive *z*-axis with low side lobe. The interior structure of RMPA is plotted in Fig. 7. Due to the presence of high dielectric constant medium (GaN ε_r 8.9, SiC ε_r 9.6), the size of the antenna will be miniaturization. Typically, RMPA composes of a microstrip-line and a rectangular patch which are optimized separately. Guided waves are confined to the microstrip-line which is used as a feed source. Then rectangular patch transmits guided waves from microstrip-line into free-space. A well-matched microstrip-line guides waves with little radiation leakage and the rectangular patch optimizes radiation.

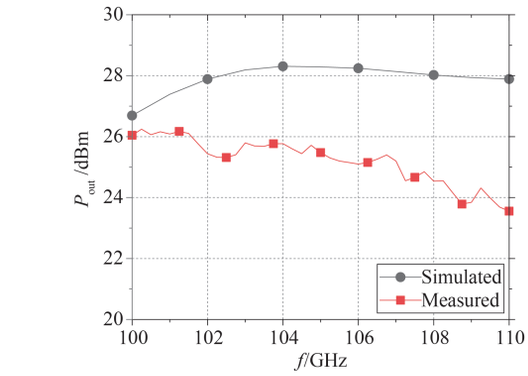

Fig. 5　Large-signal parameter P_{out}
图5　大信号参数输出功率

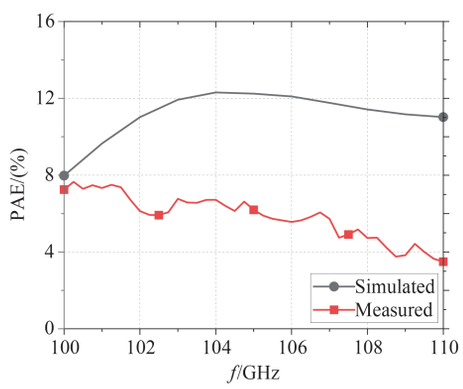

Fig. 6　Large-signal parameter PAE
图6　大信号参数功率附加效率

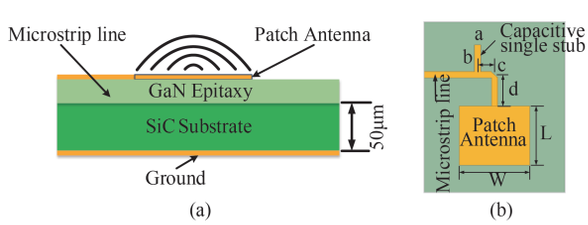

Fig.7　Interior structure of RMPA (a) side view, and (b) top view
图7　矩形微带贴片天线内部结构示意图(a)侧视图,(b)顶视图

Table 1　RMPA parameters for impedance matching condition
表1　矩形微带贴片天线阻抗匹配结构尺寸参数

Antenna parameter	Optimum value /μm	Antenna parameter	Optimum value /μm
L	415	*b*	188.5
W	500	*c*	117.85
a	3.8	*d*	221.5

The width W of the patch, marked in Fig. 7, controls the input impedance. For a patch antenna fed in the manner above, the real part of input impedance will be on the order of 130 Ω (Fig. 8(a)). By increasing the width, the impedance can be reduced. However, to modulate the impedance meeting with the amplifier's requirement, it often requires a very wide patch antenna, which takes up a lot of valuable area. A capacitive single stub is added on microstrip-line to help adjusting impedance. The specific position is calculated and designed to be away from the patch structure. This open circuit line decreases coupled effect comparing to the inductive stub.

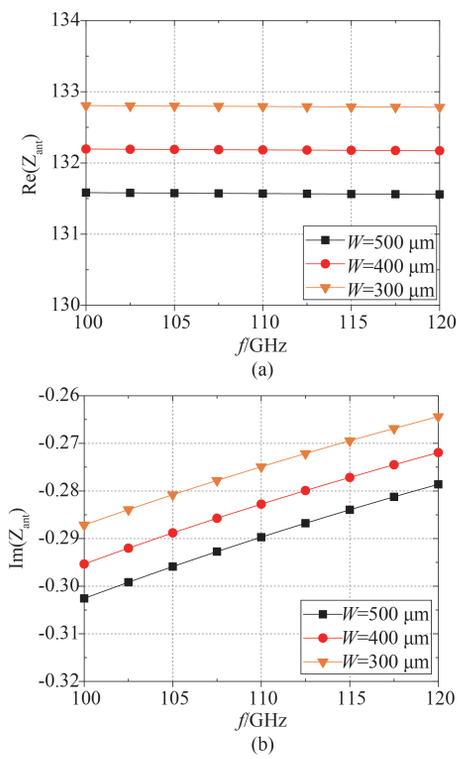

Fig.8 Optimum result of patch width W (a)real part of port impedance, and (b)imaginary part of port impedance
图8 贴片宽度W优化结果(a)贴片端口阻抗实部,(b)贴片端口阻抗虚部

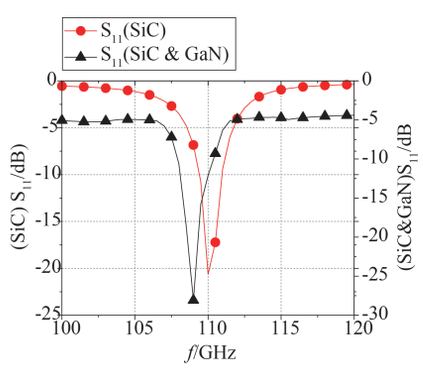

Fig. 9 Small signal S_{11} parameter of RMPA
图9 矩形微带贴片天线小信号参数S11

Some noteworthy observations are apparent from Fig. 9. Firstly, the relatively narrow frequency bandwidth can be explained by the resonant characteristic of the RMPA, which ideally radiates at single designed resonant frequency. Secondly, the antenna is designed to operate at 110 GHz on SiC substrate, and it is resonant at approximately 109 GHz when GaN material is added. This shift is due to fringing fields around the antenna and the composite dielectric material, which makes the patch seem longer. Hence, when designing a patch antenna it is typically trimmed by 2%~4 % to achieve resonance at the desired frequency.

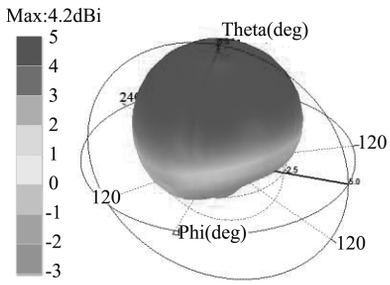

Fig. 10 Radiation pattern of RMPA
图10 矩形微带贴片天线辐射方向图

Radiation pattern is the key factor that define the performance of an antenna. The RMPA gain is approximately 4.2 dBi. Single main lobe and low side lobe can be seen when viewing radiation pattern of the antenna in Fig. 10. High gain can be obtained when single-antenna cells are combined into antenna array.

1.3 Analysis of integration between the amplifier and the antenna

In the inchoate design concept, where an antenna and an amplifier are connected by a discrete transmission line, the loss associated with the hybrid design limits the practical efficiency of the device. With the expectation of improving radiation power, the antenna is directly attached to the amplifier, allowing the antenna to serve as a radiating element and a tuned load, thus minimizing circuit size and insertion loss.

Since the output matching is critical in determining the output power and efficiency, the circuit design was carefully done. In this study, the measured Z_{ant} is directly transformed to the Z_{out} for optimum efficiency at the fundamental frequency, bypassing the conventional intermediate 50 Ω-line stage. No additional output matching network is needed to tune higher order harmonics due to the intrinsic harmonic termination characteristics of the antenna. Thus, the signal power at the fundamental frequency is radiated through the antenna while signal power at higher order harmonics is not due to the reactive termination.

The design steps [17] are described as follows.

Step one, setup simulation models for the amplifier and the antenna in ADS and HFSS, separately. Port parameters will be obtained.

Step two, extract reflection coefficient Γ_{ant} from the antenna model and calculate its impedance Z_{ant} (Fig. 11) using de-embedding method.

Step three, based on optimized stabilization and gain figures of the amplifier, source reflection coefficient Γ_S is selected and output reflection coefficient Γ_{out} is determined by S parameters in Eq. 1. The output port impedance of the amplifier Z_{out} is calculated and shown in Fig. 12.

$$\Gamma_{out} = S_{22} + \frac{S_{12}S_{21}\Gamma_S}{1 - S_{11}\Gamma_S} \quad . \quad (1)$$

Step four, port impedances of output matching networks are then designed and calculated according to the optimized Z_{out} and the antenna impedance Z_{ant} (complex impedance), respectively.

Step five, the integrated antenna reflection coefficient Γ_L can be calculated from Z_L and Z_L^* according to Eq. (2) where Z_L^* is the complex conjugate of Z_L.

$$\Gamma_L = \frac{Z_{out} - Z_L^*}{Z_{out} + Z_L} \quad . \quad (2)$$

Step six, add the antenna as a single-port device defined by an s1p file which gives the opportunity to simulate the integrated system. Radiation characteristics of the AIA will be simulated via field-circuit co-design in ADS, which enables us to run both microwave circuit and electromagnetic field simulators together.

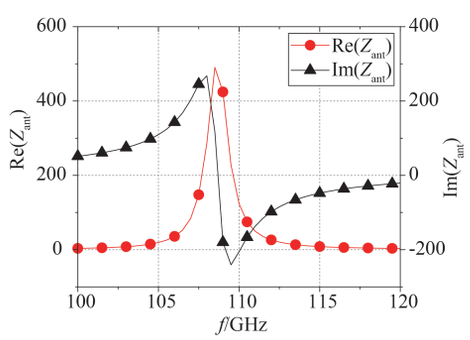

Fig. 11　Port impedance of the antenna
图 11　天线端口阻抗

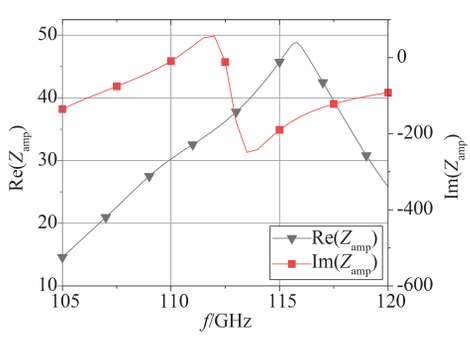

Fig. 12　Output impedance of the amplifier
图 12　放大器输出端口阻抗

The output impedance of the power amplifier was simulated and found to be Z_{amp}=30~9j Ω while the port impedance of the antenna was simulated and found to be Z_{ant}=123~205j Ω. For optimum impedance matching, the output matching network should have an impedance transformation at the desired matching based on a load-pull power-amplifier design model.

According to the description above, the RMPA and the amplifier have been designed respectively and then combined together for the TMIC. The antenna is attached to the output matching network, which is performed as an impedance matching structure.

2　Assembly and measurement

GaN HEMT power amplifier has high working voltage and working current due to its native characteristics, which will produce large power dissipation. Therefore, the material and structures with good electrical and thermal conductivity are considered and adopted in the process of chip assembly to ensure the heat dissipation.

Firstly, the TMIC is assembled on a gold-plated molybdenum copper carrier with 0. 1 mm thickness by using eutectic AuSn solder alloy sintering process. As a common chip-assembling material, the AuSn solder alloy can meet the fast heat dissipation while ensuring the good grounding performance of the chip.

Secondly, the conductive-resin bonding process is used to assemble the molybdenum copper carrier on the copper heatsink. The copper heatsink efficiently dissipates heat generated from the GaN HEMT so that accurate power performance measurements can be made. A pure silver filled, electrically and thermally conductive epoxy paste adhesive (NSP-801) is adopted. It exhibits outstanding flexibility for bonding materials with highly mismatched coefficient of thermal expansions (i. e. , alumina to aluminum, silicon to copper). The characteristic parameter is shown in Table 2.

Table 2　NSP-801 properties
表 2　NSP-801 特性

Parameters	Value	Parameters	Value
Volume Resistivity	11 μΩ·cm	Hardness	24. 11HV
Stear Strength	≥40 Mpa	Viscosity	140~200 Pa·S
Thermal Conductivity	≥150 W/m·K	CTE	8. 6×10^{-6} ℃

Finally, using chemical plating process, we cover a thin layer of gold on the molybdenum copper carrier and the copper heatsink to prevent surface oxidation. Therefore, heat transfer efficiency is improved. Because the thermal expansion coefficient of SiC and copper varies greatly, the molybdenum copper carrier provides an effective thermal expansion buffer for two kinds of materials.

For the convenience of testing, fin-line transition is introduced to transform signals from rectangular waveguide to microstrip-line on the test module. Due to the discontinuity between free space and transmission line, a mismatch occurs when free-space waves are transformed into guided waves. A rectangle slot is added at the frontend of the structure to match the input impedance. A circular tuning stub is added besides the microstrip-line to extend working bandwidth. The optimized transformation loss is below -1 dB in full working-band. The designed structure is shown in Figs. 13(a-b). The simulation re-

sult is shown in the Fig. 13(c).

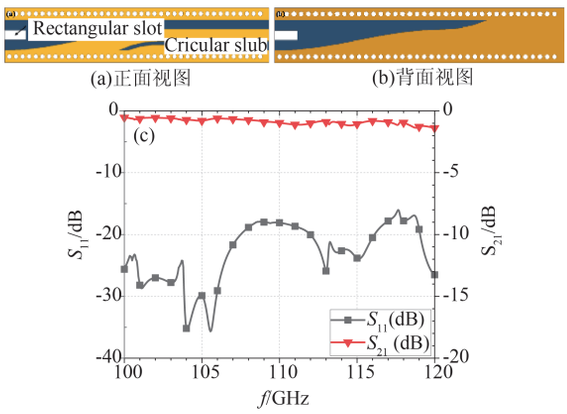

Fig. 13 Proposed fin-line structure (a) top view, (b) bottom view, and (c) simulated results of *S* parameter
图13 鳍线过渡结构(a)正面视图,(b)背面视图,(c)*S*参数仿真结果

A photograph of the fabricated GaN HEMT power amplifier integrated with the rectangular microstrip patch antenna is shown in Fig. 14.

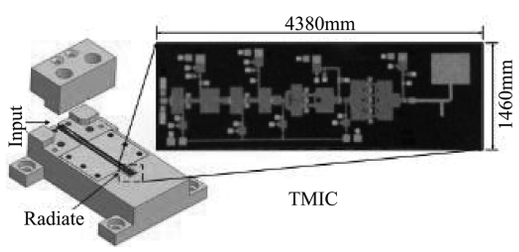

Fig. 14 Assembled structure of TMIC
图14 单片太赫兹集成电路装配示意图

Since the circuit is terminated with a radiator rather than a 50 Ω load, the measurement of this circuit is much more complicated when compared to a standard active circuit. To correctly evaluate the radiation performance of the TMIC, it is essential to calibrate the measurement setup systematically. The Friis transmission Eq. 3 is employed [18], the measurements in an anechoic chamber have been done in the following order [19-20]. First, to deem the antenna gain and mismatch loss, measurement of the passive antenna as a reference is done in the broadside direction. The passive antenna is then replaced by the power amplifier integrated with the same type of antenna and the measurement is repeated in the same direction. While compensating for the measured mismatch loss and the antenna gain from the measurement data of the passive antenna, all output performance of the power amplifier is correctly obtained. Note that, for all of these measurements, the cable loss and receiving antenna gain are accounted for as follows:

$$P_{\text{spec}} = \left(1 - \left|\Gamma_{\text{ant}}\right|^2\right) G_t \frac{P_{\text{amp}}}{4\pi R^2} \left(1 - \left|\Gamma_{\text{rec}}\right|^2\right) \frac{\lambda^2}{4\pi} G_{\text{rec}}. \quad (3)$$

In Eq. 3, P_{spec} is the power received by the spectrum analyzer (AV4051H) and represents the available power from the output of the AIA. Γ_{amp} and Γ_{rec} are reflection coefficients of transmitting and receiving antennas to quantify the mismatch losses, respectively. By considering both P_{amp} and the transmitting reflection coefficient, the delivered power to the antenna can be obtained as the output power of the GaN HEMT. In addition, G_{ant} and G_{rec} are the transmitting and receiving antenna gain. $\lambda^2/4\pi R^2$ represents free-space loss.

The radiation pattern of the TMIC was measured by using antenna far-field pattern test system. According to Figs. 15(a-b), a low frequency signal was first generated in the signal source and multiplied into 110 GHz by a terahertz-band frequency multiplier. Then, the high frequency signal was amplified and radiated by TMIC module which deployed at the center of the test system. A terahertz-band receiving horn antenna was set on a sliding rail attached to a rotating table. The distance satisfied the far-field condition. Spatial signal was received by a horn antenna and then down-converted to a low frequency by a downconverter of the spectrum analyzer. E-plane far-field pattern (Fig. 15(c)) was obtained by scanning around the TMIC module. Based on simulated 55% antenna efficiency, 25.5 dBm equivalent isotropic radiated power (EIRP) was estimated at 109 GHz. The rotating table driven by the stepping motor ensured the scanning accuracy.

3 Conclusion

The TMIC designed in this paper has the characteristics of high integration and effective output, which can realize power transmission and radiation at the same time. A TMIC module is assembled and measured in a terahertz-band far-field pattern test system. Measured far-field pattern equals with the simulated result of the patch antenna. Good agreement indicates positive development prospect and research value in realizing active antenna array and be applied to spatial power combining application.

Acknowledgment

This work was supported by the National Natural Science Foundation of China (grant 61527805) The authors would like to thank Si Liming, Liu Yong, Ni Hongbin, Qiao Haidong, and Liu Jun for helpful discussions.

References

[1] Minamide H. Development of high-power terahertz-wave sources for finding novel applications [J]. *IEEE Transactions on Terahertz Science and Technology*, 2015, **5**(6): 1104-1109.
[2] Kai C, Cheng S. Millimeter-wave power-combining techniques [J]. *IEEE Transactions on Microwave Theory and Techniques*, 1983, **31**(2): 91-107.
[3] Schoenberg J, Mader T, Shaw B, *et al*. Quasi-optical antenna array amplifiers [J]. *Proceedings of 1995 IEEE MTT-S International Microwave Symposium*, 1995, **602**:605-608..
[4] Radisic V, Qian Y, Itoh T. Novel architectures for high-efficiency amplifiers for wireless applications [J]. *IEEE Transactions on Microwave Theory and Techniques*, 1998, **46**(11): 1901-1909.
[5] Radisic V, Siou Teck C, Yongxi Q, *et al*. High-efficiency power amplifier integrated with antenna [J]. *IEEE Microwave and Guided*

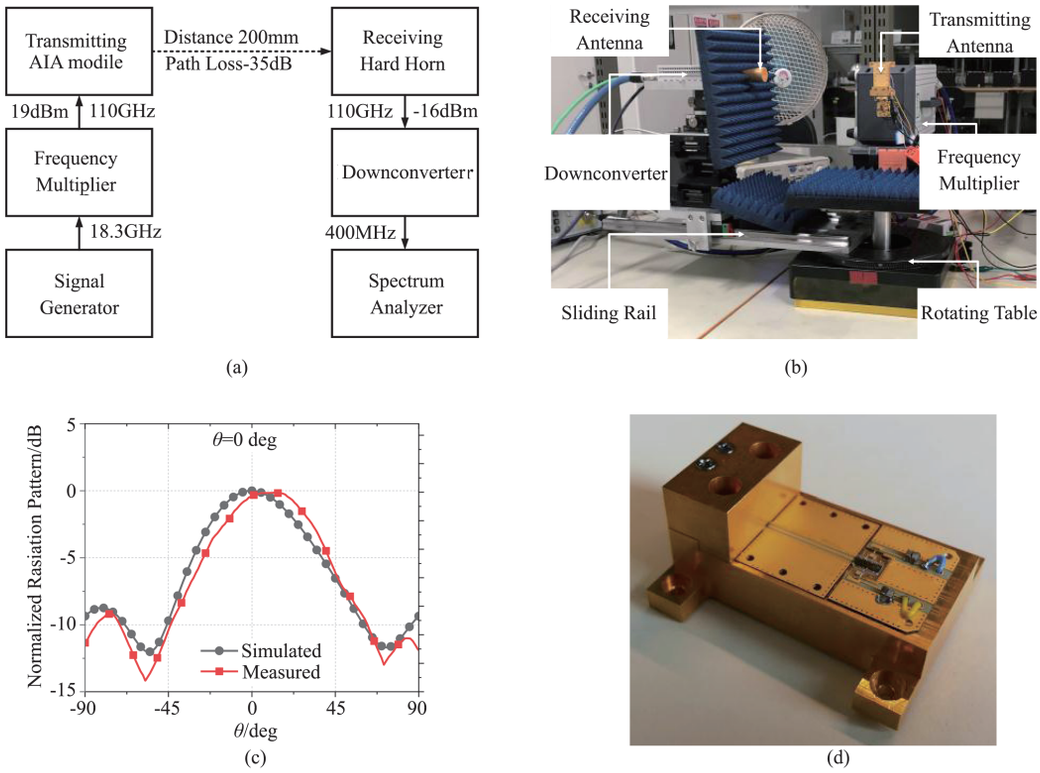

Fig.15　Measurement of the TMIC (a) far-field pattern test system schematic, (b)far-field pattern test system photograph, (c) simulated and measured radiation pattern, and (d) photograph of TMIC module

图 15　TMIC模块测试 (a)远场方向图测试系统原理图, (b)远场辐射方向图测试系统现场照片, (c)归一化的仿真与测试远场方向图, (d)模块实物照片

Wave Letters, 1997, **7**(2): 39-41.

[6] Deal W R, Radisic V, Yongxi Q, *et al.* Integrated-antenna push-pull power amplifiers [J]. *IEEE Transactions on Microwave Theory and Techniques*, 1999, **47**(8): 1418-1425.

[7] Radisic V, Yongxi Q, Itoh T. Broadband power amplifier integrated with slot antenna and novel harmonic tuning structure [J]. *IEEE MTT-S International Microwave Symposium Dugest* (*Cat. No.* 98CH36192), 1998, **1893**: 1895-1898.

[8] Yin Q, Gao S, Sambell A. Broadband high-efficiency circularly polarized active antenna and array for RF front-end application [J]. *IEEE Transactions on Microwave Theory and Techniques*, 2006, **54**(7): 2910-2916.

[9] Hyungrak K, Ick-Jae Y, Young Joong Y. A novel fully integrated transmitter front-end with high power-added efficiency [J]. *IEEE Transactions on Microwave Theory and Techniques*, 2005, **53**(10): 3206-3214.

[10] Song Y, Wu Y, Yang J, *et al.* A Compact Ka-band active integrated antenna with a GaAs Amplifier in a ceramic package [J]. *IEEE Antennas and Wireless Propagation Letters*, 2017, **16**: 2416-2419.

[11] Sarkas I, Hasch J, Balteanu A, *et al.* A fundamental frequency 120-GHz SiGe BiCMOS Distance Sensor With Integrated antenna [J]. *IEEE Transactions on Microwave Theory and Techniques*, 2012, **60**(3): 795-812.

[12] Pengelly R S, Wood S M, Milligan J W, *et al.* A review of GaN on SiC high electron-mobility power transistors and MMICs [J]. *IEEE Transactions on Microwave Theory and Techniques*, 2012, **60**(6): 1764-1783.

[13] Wang C, Xu Y, Yu X, *et al.* An electrothermal model for empirical large- signal modeling of AlGaN/GaN HEMTs including self-heating and ambient temperature effects [J]. *IEEE Transactions on Microwave Theory and Techniques*, 2014, **62**(12): 2878-2887.

[14] Colantonio P, Giannini F, Giofre R, *et al.* A C-band high-efficiency second-harmonic-tuned Hybrid Power Amplifier in GaNTechnology [J]. *IEEE Transactions on Microwave Theory and Techniques*, 2006, **54**: 42713-2722.

[15] Ćwikliński M, Friesicke C, Brückner P, *et al.* Full W-band GaN power amplifier MMICs using a novel type of broadband radial stub [J]. *IEEE Transactions on Microwave Theory and Techniques*, 2018, **66**(12): 5664-5675.

[16] Krishnamoorthy R, Kumar N, Grebennikov A, *et al.* A high-efficiency ultra-broadband mixed-mode GaN HEMT power amplifier [J]. *IEEE Transactions on Circuits and Systems II: Express Briefs*, 2018, **65**(12): 1929-1933.

[17] Dhar S K, Hammi O, Sharawi M S, *et al.* Power amplifier based integrated and miniaturized active antenna [C]. *In European Conference on Antennas and Propagation* (*Eu CAP*), 9th, 2015: 1-4.

[18] Balanis C A, *Antenna Theory: Analysis and Design* [M]. New York: Wiley, 1997.

[19] Radisic V, Qian Y, Itoh T. Novel architectures for high-efficiency amplifiers for wireless applications [J]. *IEEE Transactions on Microwave Theory and Techniques*, 1998, **46**(11): 1901-1909.

[20] Hang C Y, Deal W R, Yongxi Q, *et al.* High-efficiency push-pull power amplifier integrated with quasi-Yagi antenna [J]. *IEEE Transactions on Microwave Theory and Techniques*, 2001, **49**(6): 1155-1161.